1 Title: Variations of permafrost under freezing and thawing conditions in the coastal catchment
2 Fuglebekken (Hornsund, Spitsbergen, Svalbard)

3 Authors: Majdański Mariusz[1], Dobiński Wojciech[2], Marciniak Artur[1], Owoc Bartosz[1], Glazer Michał[2],
4 Osuch Marzena[1], Wawrzyniak Tomasz[1]

5 1) Institute of Geophysics, Polish Academy of Sciences, Warsaw, Poland
6 2) University of Silesia, Faculty of Natural Sciences, Sosnowiec, Poland

7 Corresponding author: Majdański Mariusz, mmajd@igf.edu.pl

8

9 Abstract

10 Two seismic field surveys were organized in the Fuglebekken coastal catchment of Hornsund,
11 Spitsbergen, Svalbard, to map frozen and unfrozen ground and assess the spatial and temporal state
12 of the permafrost. Surveys were conducted during maximum thawing in September and maximum
13 freezing in April of the following year. The obtained seismic wavefields were interpreted using three
14 methods: the surface waves dispersion, seismic refraction, and traveltime tomography. The seismic
15 experiments were supported by nearby boreholes with continuous thermal monitoring. In the frozen
16 survey, a gradual increase in ice content of water-filled sediments was found, further from the coast.
17 In September the shallow sensors in the boreholes validated positive ground temperatures down to
18 3.0 m depth, with below zero temperatures at greater depths. However, the seismic tomography
19 indicated that the ground was unfrozen down to 30 meters. The ground probably remained unfrozen
20 due to intrusion of high salinity seawater, even though it had been below 0°C. In April, in the area 300
21 m and farther form the coast, the ground below 3 m depth was frozen, except for a 19 m deep open
22 talik identified in a borehole at the slope of Fugle Mountain. We attribute the complex spatial extent,
23 form, and condition of permafrost in the Fuglebekken coastal catchment to multiple factors, including

variable solar energy, snow and ground cover, thermal and humidity properties of the soil, subsurface water flow, and seawater intrusion. The presented combination of seismic methods provides a new robust and precise approach to access spatial variability of permafrost in a coastal environment. The proposed interpretation show deep percolation of subsurface flow into permafrost and it's seasonal unfreezing at a depth of 30 m in both saltwater intruded zone and the slope area.

1. Introduction

Permafrost plays an important role in high latitude and altitude ecosystems, underlying 25% of the terrestrial parts of Earth (Christiansen et al. 2021). The thermal state and changes of permafrost is a crucial indicator of environmental changes occurring in the Arctic. In Svalbard permafrost underlies almost all land areas that are not covered by glaciers. Changes in climatic variables, especially the air temperature, snow depth, and the increased duration of the period with positive air temperature have resulted in an increase of permafrost temperature and deepening of the active layer (Christiansen et al. 2021).

In SW Spitsbergen, Svalbard, the changes in air temperature observed at the Hornsund meteorological site over the last four decades (1979–2018) are more than six times higher than the global average (Wawrzyniak and Osuch 2020). Degradation of permafrost results in a change in hydrogeological and geotechnical properties of the ground, hydrological and biogeochemical processes, landforms, and other components of the ecosystems. The thickness of the active layer, that increased globally from 0.2 to 1.0 m in the last four decades, is expected to increase, especially in the Arctic due to the polar amplification (IPCC 2019).

Ground thermal conditions in the vicinity of Ny-Ålesund, Longyearbyen, Barentsburg, Kapp Linné, and Hornsund were described by Christiansen et al. (2019a, 2020), in Petuniabukta by Rachlewicz and Szczuciński (2008), in Bellsund by Marsz et al. (2013), and in Kaffiøyra Plain by Sobota and Nowak (2014). Lowland permafrost is at temperatures close to 0°C making it very sensitive to climatic change.

Moreover, the warmest permafrost in Svalbard has been found in Hornsund. Temperatures observed at a depth of 12 m are only -1.1 °C on average (Christiansen et al. 2019b, 2020). Unfortunately, in situ point monitoring of the ground thermal state is insufficient to evaluate the spatial variability of permafrost thickness. Spatial heterogeneity of the thaw depth is influenced by the local solar and atmospheric conditions, ground surface albedo, exposure, thermal and humidity properties of the soil, thickness and duration of snow cover and vegetation, and the depth of permafrost itself (Christiansen et al. 2020).

Geophysical measurements, apart from thermal monitoring, cannot measure the temperature of the subsurface directly, but they can indirectly detect changes in physical parameters and properties of the ground. Laboratory analysis shows that at temperatures exceeding 0 °C the rocks with low porosity, experience a significant (ca. 11%) increase in seismic P-wave velocity when compared with the same rocks in negative temperatures (Draebing and Krautblatter, 2012). This is sufficient to identify the presence of permafrost within a single rock unit (Hauck and Kneisel, 2009). Locally, where the velocity, lithology and distribution of rocks do not vary significantly, such a change at the edge of permafrost can certainly be detected by seismic methods, even at great depths. The P-wave velocity in high porosity rocks will double after freezing (Draebing 2016; Carcione and Seriani 2001; Dou et al. 2014). Recent scientific efforts have focused on studying permafrost in high mountains and polar regions using a variety of geophysical methods, including gravity measured by satellite (Gido et al., 2019), Electrical Resistivity Tomography (Minsley et al. 2012; Dobiński 2011), Surface Waves Analysis (Tsuji et al. 2012; Rossi et al. 2017), Travel Time Tomography (Hilbich 2010), shear waves (Lecomte et al., 2014), and Reflection Seismic Imaging (Strobbia et al. 2009; Johansen et al. 2003, 2011; Oye et al. 2013). However, little information is available about the impact of active layer seasonal changes on seismic wavefields. Most research has been conducted during the summer thawing conditions. Seismic measurements have been performed on Svalbard in Adventdalen, including imaging of deep structure to store C02 safely (C02 Lab; Baelum et al. 2012). These experiments showed that the high spatial precision imaging is possible down to 1 km.

Periglacial studies have been conducted in the Hornsund area since the 1950s, resulting in a description of the geomorphological characteristics of this area (Baranowski 1968), and the long-term measurement of the near-surface ground temperature (up to 1 m) was initiated in 1978 at the meteorological site of the Polish Polar Station (Wawrzyniak et al. 2016). The post-glacial evolution of the Hornsund coast, which is also important for the development of permafrost in this area, was described by Pękala and Repelewska-Pękalowa (1990). The thermal state of the ground and active layer thickness in the Hornsund area have been discussed in several studies. Jahn (1982, 1988) and Grześ (1984) analysed soil structures and permafrost-related geomorphological processes. Migała (1991, 1994) and Dolnicki (2005) described the influence of snow cover on ground temperatures. Miętus (1988), Miętus and Filipiak (2001), Leszkiewicz and Caputa (2004), and Dolnicki (2010, 2013) described variability of the active layer thickness in the Hornsund area. Dobiński and Leszkiewicz (2010) analysed permafrost occurrence by the first application of geophysical methods in the vicinity of Hornsund and indicated the possibility that water can penetrate deeply into the ground and interact with permafrost. The thermal regime of permafrost in Hornsund was studied by Wawrzyniak et al. (2016). The permafrost state in the vicinity of the PPS Hornsund was modelled using the numerical heat transfer model CryoGrid 2, which was calibrated with borehole data and validated with available observations from the period 1990-2014. The simulated subsurface temperature indicated that multiannual variability in that period can reach 25 m in depth.

Further, ERT studies in this area showed a relationship between soil structure and the permafrost table (Kasprzak 2015), but also found an effect of seawater on the coastal permafrost, imaged as a permafrost wedge in the near-surface onshore permafrost (Kasprzak et al. 2017), and described the active layer in the coastal permafrost (Kasprzak 2020). Finally, thanks to a combination of ERT and MASW techniques, the occurrence of permafrost was recognized in the Hornsund area with a distinction between ice-free, ice-bearing, and cryotic permafrost (Glazer et al. 2020).

This study aims to analyse the applicability of seismic methods, surface wave dispersion, seismic refraction and traveltime tomography, to obtain new high-resolution information of key permafrost characteristics in deglaciated areas. Due to the prevalence of climate warming, the form and condition of permafrost are changing that it requires additional validation in the studied area. High spatial resolution in the imaging of the velocity field of the seismic method and direct monitoring of ground temperature allow validation of the hypothesis that a wide extent of unfrozen ground exists proximal to the coast, likely influenced by saltwater intrusion and mineralization of the groundwater (the cryotic state; Dobiński 2020). Seismic studies can also provide information about the thickness of the active layer and be compared with the distance to the shoreline, elevation, and the presence of streamwater. Another interesting interface is the boundary between the sedimentary material and the solid rock beneath it. In these two media the seismic wave velocities can be different, and, in addition, can change seasonally depending on the depth at which the ground freezes. Our study, based on two surveys in the spring and late summer, estimates the minimum thaw depth and active layer thickness, the depth of surface temperature influences on the permafrost, and the extent of permafrost in the coastal catchment Fublebeckken. We show links between the permafrost characteristics (frozen and ice bearing zones) and the distance to the coast, slope and geology. We rely on a time-lapse seismic image, results of previous ERT survey (Glazer et al. 2020), and in-situ borehole data to conduct this study.

2. Methods – two Arctic surveys

2.1 Fuglebekken – Geological setting

The study site, the Fuglebekken coastal catchment, is located on the northern shore of Hornsundfjord, in the vicinity of the Polish Polar Station Hornsund (SW Spitsbergen, see Fig. 1). The region is underlain by Precambrian basement rocks, which arepart of the Lower and Middle Hecla Hoek succession. The crystalline basement of metamorphic quartzites, schists, paragneisses, marbles, and amphibolites is covered by Cambrian and Ordovician sedimentary successions containing a mixture of sand and gravel

with clay (Czerny et al. 1993). The Fuglebekken catchment (1.27 km^2) is heterogeneous in terms of land cover and topography and occupies the southern slopes of the Ariekammen-Fugleberget mountain ridge and the elevated marine terraces of the Fuglebergsletta coastal plain. The slopes are covered with washed rubble sediments, solifluction tongues, rock streams, alluvial cones, and bare solid rock. The bottom of the slope is covered with sea gravel, sediments, and diverse types of tundra vegetation. The hydrographic cover includes several tributaries of Fuglebekken Stream, which drains into Isbjørnhamna Bay (Osuch et al. 2019; Wawrzyniak et al. 2021). Glazer et al. (2020) and Humlum et al. (2003) provide a detailed history of the permafrost in the area during the Holocene, from the mountain region through the system of elevated marine terraces, due to marine incursions.

2.2 Thermal monitoring

To verify the results obtained using seismic methods, three shallow boreholes were drilled in April 2018, down to 20 m (Borehole 1), 5 m (Borehole2), and 10 m (Borehole 3) as presented in Figure 1 and Figure 2. Boreholes were located at previous monitoring sites, but our seismic data was acquired along with the previous ERT survey line. As a result, only Borehole 1 lies on our seismic line, whereas Borehole 2 is 100 m from the seismic line, and Borehole 3 is 250 m from the seismic line. Those out-of-line measurements cannot be directly compared with seismic data. The studied structures are complex and a variety of factors, such as geomorphology, sedimentary structure, water content and snow cover, contribute to the permafrost variability. They are presented to show termal state and its temporal dynamics in this small area. Due to environmental restrictions, the operation of heavy equipment is allowed only on thick snow cover, therefore boreholes were drilled during the second survey. Automatic sensors (Geoprecision M-Log5W) were installed at irregular intervals from 0.2 to 20 m (maximum 18 sensors in a single borehole) to measure ground temperatures in the active layer and permafrost. In addition to thermal measurements, piezometers were installed to measure the depth of groundwater level as far as 5 m below the surface. Hourly measurements were recorded for

different periods from installation: Borehole 3 (12 days), Borehole 2 (7 months), Borehole 1 (17 months and still active).

The thermal data were interpolated and are presented in Fig. 2. The longest series (17 months) collected in Borehole 1 shows seasonally repeated heat transfer down to 4 m. Extreme temperatures were recorded by the shallowest sensor (at a depth of 20 cm), reaching +16 °C on 28 July and -19 °C on 21 January 2019. Surprisingly, 0 °C was observed at a depth of 19 m. The behaviour of Boreholes 1 and 2 was found to be closer to expectation, with heat waves reaching 2 m and continuous sub-zero temperatures below that depth, similar to the results described by Kasprzak et al. (2017). Fig. 2 also shows air temperatures measured at the Polish Polar Station Hornsund (Vaisala QMT107) with the dates of both surveys marked (red and blue lines). As borehole measurements were not available during the first survey, and the cycle repeats annually, the temperatures from September of the subsequent year were used in further analysis.

The fact that Borehole 3 was made at the end of winter is particularly noteworthy as the temperatures recorded are relatively high, ranging from about -3 °C at the surface to about -0.5 °C at a depth of 10 m. Still, Borehole 3 recording was operational for only 12 days and located too far from the line to allow reliable calibration of seismic data. It should be added that during the drilling, the ground, except for a thin layer at the surface, was not frozen. The most surprising temperature profile of the ground was found at Borehole 1. The 16-month sequence of temperatures revealed that seasonal freezing reaches a depth of 8 m, but the summer thaw is much deeper. In July and August 2018, in particular, a sharp increase in temperature was visible, reaching 12–18 m. This is interpreted as an evidence of a strong underground flow that percolates deep into the ground, resulting in the occurrence of an extremely deep active layer at this site, ranging from about 18 m in 2018 to almost 20 m in 2019. This is one of the few places in the world where the active layer reaches such a thickness. In addition to that detected in Hornsund, a similar depth has also been recorded in the Rocky Mountains and Labrador (Dobiński 2020).

2.3 Two active seismic surveys

For the first time in SW Spitsbergen, a multi-method approach was applied to reveal the spatial distribution of frozen ground and the active layer. Most permafrost studies in the High Arctic are conducted in the summer season because of the availability of daylight and easier logistics. Two fieldwork campaigns were conducted at different seasons: (a) during ground at maximal thaw (21-28 September 2017, Unfrozen survey) and (b) during maximum snow cover with minimal thaw (15 April – 10 May 2018, Frozen survey). The seismic data were collected twice on the same profile located between the seashore and the mountain slope (see Fig. 1). Sixty standalone seismic stations (DATA-CUBE, Omnirecs) with 1C 4.5 Hz geophones in walking spread deployments were used to obtain a high-resolution near-surface seismic dataset. The survey was designed to provide the longest offsets for observations without sacrificing resolution (see Fig. 3 for details). For the first survey, both receivers and sources were deployed every 2 m (each source was stacked 3 times), in the second survey the receivers were positioned every 5 m and sources every 2.5 m (each source was stacked 6 times, because of longer offsets). Attenuation of the seismic waves in frozen ground is significantly lower; thus it is possible to observe refraction at a much larger offset. Changing receiver spread to 5 m gave a maximum of 350 m offsets. Additionally, 20 m of overlapping shot locations were established. The PEG-40 accelerated weight-drop with 40 kg of usable mass was used as a seismic source. The seismic signal was generated by striking a steel plate. An additional strike was made before the actual acquisition of data for each shot point to compact the ground and snow cover. The seismic source was mounted on an in-house built cart, and a sledgehammer (8 kg) was used as the source in places that were difficult to access during the first survey.

In the second survey, during maximum snow cover, the seismic source was mounted on a sledge. In this open terrain, the snow cover was in a range from 0 to 0.4 m. Both devices were equipped with power generators and a GPS-based timing system designed in-house (timing dispersion of less than 2 ms) to determine the excitation time. Precise source timing enabled correct vertical stacking to be

197 achieved, resulting in a high signal-to-noise ratio. Measurements at the level of the snow caused a
198 large mismatch of the time of the first strike due to snow compaction, thus, all the first strikes recorded
199 had to be discarded from the vertical stacking. The elevation data was gathered from the DTM model
200 based on laser scanning (Riegl system) and GPS measurements.

201 2.4 Recorded seismic wavefields

202 Seismic records from separate deployments (see Fig. 3) were merged into a single dataset, after
203 manual quality control, vertical stacking, and adding geometry information. An example of a seismic
204 wavefield recorded from the same shot location during both surveys is presented in Fig. 4. There are
205 clear arrivals at all measured offsets that were longer in the frozen ground during the 2018 survey due
206 to a change in the acquisition method (larger receiver spacing, resulting in an elongation of the profile
207 using the same number of sensors). Both P-wave and S-wave refractions are visible at large offsets in
208 both surveys. In near-surface applications, near-field observations (offsets shorter than 20 m) are
209 difficult to perform for P-waves, and not possible for S-waves. Also, clear wide-angle reflections are
210 visible at larger offsets. In the unfrozen conditions (in 2017) surface waves were the strongest signals
211 in the wavefield, while in the frozen survey in 2018 they were observed only for several shots at rocky
212 outcrops without snow cover. In these conditions even thin snow cover suppresses surface waves.
213 However, high-amplitude, non-dispersive S-wave refractions were observed. Shot gathers of long
214 offset refractions (Fig. 4) show P-wave velocities (Vp) of 3500 m/s in unfrozen and 5200 m/s in frozen
215 conditions, both with uncertainty ±100 m/s and of 1300 m/s and 2300 m/s, respectively, for S-wave
216 velocities (Vs), with uncertainty ±150 m/s. Only apparent velocities are measured, not including layer
217 thickness and dipping layers from a single gather. Even so, the seasonal difference is very large, almost
218 doubled, confirming the laboratory observations made by Draebing (2016).

219 2.5 Near-surface techniques – MASW and seismic refraction

Multichannel analysis of surface waves (MASW, Park et al. 1999) is a well-known technique that is sensitive to changes in shear velocity (Vs) in the shallow subsurface. This technique is also known to be difficult to apply to complex structures due to its low precision. As surface waves were occasionally recorded in the frozen ground survey, only results from the unfrozen survey are discussed. Globe Claritas and Geopsy software were used to calculate the classic inversion of the surface waves dispersion curve for 30-channel data blocks resulting in eleven 1D Vs profiles. To limit the near-field effects, short offset channels (<20 m) were not used in the analysis. Also, all refraction and reflection signals were muted or filtered out of the data using a 2-50 Hz bandpass filter to increase the visibility of surface waves and thus enhance the dispersion curve. The results (Fig. 5, top) present a consistent strong Vs contrast between the layers, the top layer with an average velocity of 300 m/s and the lower with an average velocity of 1300 m/s, visible at a depth varying from 3 to 16 m with average uncertainty of ±1 m. The velocity uncertainty is estimated as ±100 m/s in the top layer and is much larger (±500 m/s) in the bottom layer. This strong contrast is the boundary between fluvial sediments and compacted bedrock. The 1D results also show a much weaker, but consistent, change in Vs from 200 to 300 m/s at 0.5–4 m depth. This corresponds to the underground water table that was determined by the piezometers in the borehole 1. Moreover, stream water at the surface was also observed in this area at a distance of 330–430 m of the analysed profile, where this change is not visible in Vs. Figure 5 shows the interpolation of 1D results into a pseudo-2D Vs model.

The second near-surface technique employed was the analysis of short-offset P-wave refraction arrivals (details in Schrott and Hoffmann 2008). Because of the complex structure along the profile, including rocky outcrops, a stream, and varying levels of the water table, an initial model for inversion was created using 1D analysis at eight regular intervals, separately (Fig. 6 top). Observations from the unfrozen survey clearly show a rapid change in Vp velocity at about 10 m, confirming the depth to bedrock described using MASW with higher precision (Fig. 6). The 2D models, for both seasons, were calculated using all the refraction observations for offsets smaller than 40 m, generating the detailed shape of the bedrock (Fig. 7a,b). The independent results from the two seasons described an almost

identical shape for the bedrock, confirming it is a lithological, not a thermal, feature. The Vp in the sediments changed significantly between the seasons, with an average of 1500 m/s in the unfrozen survey reaching over 5000 m/s in the frozen survey. Moreover, in the unfrozen state, all Vp along the profile were similar, while the frozen survey found significant differences depending on the distance from the coast. Close to the coast (up to 120 m away), the medium remained partially unfrozen, with Vp 3500 ±100 m/s, while further away it was fully frozen (Vp > 4500 ±100 m/s).

More importantly, a change in Vp is also visible in the bedrock; in the unfrozen survey, bedrock Vp ranged from 3300 to 5500, while in the frozen survey all Vp were higher than 5000 m/s. Both near-surface techniques using P and S-waves provided independent information about the thickness and internal velocity structure in the sedimentary layer and just below the boundary. However, both methods are useful only at shallow depths.

2.6 Ray-based refraction tomography

To reach lower depths and utilize all refraction observations, it is necessary to use refraction traveltime tomography. Ray-based JIVE3D code (Hobro et al. 2003) was used to identify velocity distribution in this study. The seismic refraction results were used as an initial model for tomographic inversion. Inversion results for both seasons are presented in Fig. 7c,d with uncertainty analysis in Fig. 7e,f.

The greyed-out areas are just the results of inversion smoothing and are not confirmed by seismic ray coverage. Both results show dense crystalline material with large Vp at distances of 200 m (corresponding to the rocky outcrop at the surface) for the basement and loosely compacted rock in the centre of the profile (330–430 m). The uncertainty of the tomographic velocities was estimated using the statistical analysis of 121 randomly generated starting models (as in Owoc et al. 2018). The uncertainty associated with the frozen survey is very good (ca. 50 m/s) down to 40 m, due to the large data set (2.5 m spacing), and for unfrozen survey the uncertainty is acceptable (<400 m/s) down to 30

m. It would be possible to perform a similar analysis of S-waves, but due to the lack of short offset observations, such results would be highly uncertain.

3. Results and discussion

The obtained methodical results provide new information regarding recognition of permafrost variability, facilitating better planning and future adaptation of the measurement methodology. In addition, the results of the research deliver new information regarding the occurrence of permafrost on the Spitsbergen coast.

3.1 Optimal seismic refraction survey

Fieldwork in the polar regions is always challenging. In the case of studies of the active layer, the period from August to September seems optimal, as evidenced by the borehole thermal data. During these months, the thawing of the active layer is almost maximal, and seismic studies based on surface waves and refractions are feasible. The use of lightweight seismic sources makes it possible to generate seismic waves that can easily be observed at 300 m offsets, resulting in the recognition of structures down to 40 m. Moreover, a 2 m spacing of sources and receivers, and a dominant refraction frequency in the range of 30–100 Hz, provides a precise characterisation of the active layer. However, investigations of the deeper structure are significantly simpler to conduct during the winter, when stronger seismic sources can be used on snow. Due to environmental restrictions heavy duty equipment cannot be used in open tundra areas. Moreover, the presence of a frozen active layer is optimal for deep seismic studies, where waves are not attenuated in near-surface layers. However, as shown in this case study, surface waves were only occasionally observed in the wavefield from the frozen period, making the use of the MASW method impossible.

Due to environmental restrictions, only non-invasive seismic sources are allowed, which automatically limits the possibility of using strong sources. For this reason, a good methodology for gathering and

processing data from relatively weak sources is necessary. As shown, the uncertainty-driven approach (see also Marciniak et al. 2019), which combines different seismic waves with independent information, seems to be an effective way to obtain results from such demanding datasets.

3.2 Characteristics of permafrost and its relation to ground temperature

The results obtained for the near-surface structures were integrated and are presented in Fig. 8 with the estimated thermal state of the ground, obtained from nearby boreholes. The most notable feature is the sharp contrast in velocities, for both Vp (1500 to 4000 m/s) and Vs (300 to 1300 m/s), located, on average, 10 m below the surface. This interface has been interpreted as a lithological boundary between water-filled unconsolidated and consolidated rocks. The seasonal change of seismic velocities is significant between seasons. On average, the Vp in the sediments was 1500±50 m/s in the unfrozen state and 4500±100 m/s in the frozen state. Such a spread suggests (after Draebing 2016) the presence of high porosity and water-saturated fractured metamorphic rocks or a mixture of sand and clay.

As predicted by Gregersen et al. (1983) and Christiansen et al. (2010), a strong effect of seawater on the freezing of sediments is visible for the frozen survey. At a distance of 150 m from the coast, a rapid change of Vp was observed (Fig. 7d). The Vp in the section from the coast to around 150 m is significantly lower than in the further part of the profile. Such results indicate that the sediments did not freeze entirely. Based on air temperature measured in nearby Polish Polar Station and Borehole 3 that was 250 m out-of-the-line we could suspect that the temperature of the ground was lower than 0 °C. Although the distance from the coast line and the elevation for Borehole 3 are similar to those of the relevant part of the seismic line, a direct comparison of those states is not allowed. A variety of factors, including geomorphology, snow cover and water content, affect a local thermal state. To validate the thermal state of the ground it is necessary to have borehole measurement exactely on the seismic line. Probably this area did not freeze due to the relatively high salinity level of the seawater penetrating the ground. A comparison of Vp in the first 150 m of the profile (Figure 7c,d) shows a change between seasons (Vp 1500 to 2000 m/s with the uncertainty of 50 m/s) that has been

317 interpreted as a change in the amount of ice in the sediments. The active layer, in which temperature
318 is seasonally positive, lying on top of the cryotic permafrost but its thickness can only be established
319 by direct temperature measurement. Further, between 150 and 300 m from the coast, a strong velocity
320 gradient (2000-4500 m/s) was observed in the sediments as a result of the lower salinity of the water
321 that penetrates the ground and a gradual increase in the ice content of the medium. Salt in the ground
322 lowers the freezing point. Therefore, the ground may be below zero Centigrades temperature but not
323 frozen due to salt content. Ice-free subsea permafrost was also reported by other authors (Millero et
324 al., 2008). At distances greater than 300 m from the coast the sediments were fully frozen. There was
325 no influence of seawater and the ground was frozen at 0 °C. In such conditions, seismic methods can
326 easily distinguish the boundary between the active layer and permafrost. The characteristic velocity
327 (Vp) of unfrozen, water-filled sediments is 1500 m/s. In frozen conditions, it is 4500 m/s for sediments,
328 and 6500 m/s for a frozen solid rock. A small-scale talik, which was identified at 10 m during the drilling
329 of Borehole 1, represented an exception since it did not freeze in either season. This talik formed as a
330 result of the underground runoff generated by the steep mountain slope and the stream that exists in
331 the area in the summer, so it is classified as a hydrothermal, noncryotic talik. Surprisingly, the bedrock
332 at depths greater than 10 m also demonstrated significant variations in velocity, proving that the
333 medium may undergo seasonal freezing and thawing at such a depth. The Vp of the bedrock changed
334 from 3500±50 m/s to 6500±400 m/s between seasons, suggesting they comprise mica schists or
335 plutonic rocks, such as granite (Draebing 2016). Moreover, significant changes in velocity, larger than
336 the estimated uncertainty, occurred at a depth of 30 m. This result is similar to observations in
337 Adventdalen where ground freezing in the late summer was recognized at a depth of 50 m (Albaric et
338 al. 2021). Lower velocities are, most probably, the effect of the deep groundwater circulation also
339 visible in Borehole 1 (Fig. 2). Due to the uncertainty associated with the tomographic technique,
340 changes deeper than 30 m cannot be confirmed, and the depth at which the medium was not affected
341 by seasonal freezing changes remains unknown. Similarly, a change in Vs from 1300 m/s to 2300 m/s

342 was observed below the interface. The Vs in the frozen active layer cannot be confirmed, because of
343 the lack of surface waves in the observed wavefield.

344 Figure 8 also presents the ERT result with the MASW-based interphase (modified after Glazer et al.
345 2020). Due to the deployment used and the high resistivity contrasts of the near-surface, structures in
346 the resistivity model of the study area (Fig. 8) do not reflect exact lithological boundaries. The profile
347 was designed to observe changes in the horizontal characteristics of the permafrost within the
348 Fuglebekken. Supporting information from the results provided by MASW allowed a qualitative
349 interpretation of subsurface resistive structures in terms of ice content. Interpretation of geological
350 information below the high-resistivity ice-bearing permafrost structure is very limited, due to current
351 penetration being insufficient over long distances. Based on data from ERT, permafrost with the frozen
352 medium was found to be absent from up to approx. 250 m of the profile (Fig 8) and the extent of the
353 saltwater intrusion within the Fuglebekken catchment area was suggested to cover up to 450 m of the
354 profile (Glazer et al. 2020).

355 Thermal monitoring was active for different periods for each borehole. The thermal profiles marked in
356 Fig. 8 show the ground temperature during the frozen survey (blue lines). The ground temperature in
357 the unfrozen season, measured in the consecutive year, also reflects similar conditions taking into
358 account the air temperatures measured in this area (see Fig. 2 top). Correlation of the seismic results
359 with the thermal conditions was not possible for out-of-the-line boreholes. The shallow central
360 borehole (2), with a depth of 5 m, retained a constant temperature below 2 m in both seasons. The
361 surface stream observed in the unfrozen season carries large amounts of warm water which heats the
362 ground. The identified subsurface flow is preventing freezing, by constantly replacing groundwater by
363 the movement and transfer of heat.

364 The thermal measurements in the last borehole (1), at the bottom of the mountain slope, were
365 unusual. A negative temperature was observed down to 8 m in the frozen season, while in the unfrozen
366 season the ground had a positive temperature (max 2 °C at 4 m) down to a depth of 19 m. Such a

situation is not typical for the thermal state of the active layer but is the effect of an underground flow, which was unexpectedly observed at 10 m during drilling in the frozen season (May). This strong flow on the mountain slope heats the ground significantly during the unfrozen season. Unfortunately, the deep talik identified by measurements from the borehole is below the resolution of the seismic image, as this location is at the edge of the seismic profile.

4. Conclusions

The presented results have demonstrated that the application of multiple seismic methods (MASW, seismic refraction and travel time tomography) together with borehole data provide new high-resolution supporting observations and insight into the permafrost state. The borehole data shows the local ground thermal regime, high spatial variability and allowed us to distinguish areas with ground temperatures below and above 0 °C. Seismic methods used in time-lapse mode recognize frozen and unfrozen ground, and changes in water content. Comparing the observations from two seasons we see a significant impact of seasonal changes in the active layer on the seismic wavefield. An analysis of the short offset refractions clearly shows that the thickness of sediments and the top of bedrock are not changing in time. The travel time tomography detects the seasonal variability of seismic velocities due to partial or complete freezing of water in the medium. MASW cannot be used in time-lapse mode as the surface waves are only occasionally observed in area covered by snow. There are large differences between outcomes of the in-situ borehole data and the seismic analyses due to salinity or mineralization of water. Salt in the ground lowers the freezing point. Therefore, the ground at a temperature below zero Centigrades may be not frozen due to the salt content. The ice-free subsea permafrost was also reported by other authors (Millero et al., 2008).

Determining the boundary characteristics of the permafrost environment in the area under study is difficult via seismic methods used in this studyfor the following reasons:

- The boundary between the active layer and the permafrost beneath it overlaps the boundary between sedimentary and bedrock material.
- Marine and glacial sediments fill the spaces between the paleoskerries in the studied area very unevenly, causing the active layer to end in both sedimentary material and solid rock. This is indicated by the seismic velocities along with their seasonal variation in both the sedimentary material and the solid rock.
- in the area characterised by cryotic permafrost, it is only possible to distinguish between the active layer and the permafrost by directly measuring the temperature in the ground

However, time-lapse geophysical observations show that the characteristics of the cryotic permafrost are changing in time, which is interpreted as being due to changing amount of ice in the ground. In the Hornsund region, we are dealing with a complex form of permafrost, which is produced by a diverse set of factors. This environment is a good analogue to other coastal permafrost environments, which also likely exhibit such complexities, but Hornsund region, as the entire region of southern Svalbard, experience the fastest climate change in the Arctic. For this reason, the Hornsund region can serve as a specific example of permafrost degradation and act as a kind of field laboratory where permafrost degradation is clearly visible. As shown, the water-permafrost interactions has a significant effect that is expected to grow in the future, further increasing the slope processes and resulting in larger geohazard.

Permafrost occurring on the sea coast of Hornsund is subject to rapid degradation. We interpret this degradation to be caused by the following factors: the rapid increase in air temperature, intrusion of seawater into the shore (which is no longer subject to freezing but remains in a cryotic state), and the deep penetration of freshwater into the fractured bedrock.

Acknowledgements

This research was funded by the National Science Centre, Poland (NCN), Grant UMO-2015/21/B/ST10/02509. Jarosław Grzyb, Adam Nawrot and Wojciech Gajek are thanked for their fieldwork assistance. We thank associate editor Seth Campbell, as well as an anonymous reviewer for many comments and suggestions that improved the manuscript.

References

Albaric J., Kuhn D., Ohrnberger M., Langet N., Harris D., Polom U., Lecomte I., Hillers G., 2021, Seismic monitoring of permafrost in Svalbard, Arctic Norway, Seismological Research Letters, doi: 10.1785/0220200470.

Baelum K., Johansen T.A., Johnsen H., Rod K., Ruud B.O., Braathen A., 2012, Subsurface structures of the Longyearbyen C02 Lab study area in Central Spitsbergen (Arctic Norway), as mapped by reflection seismic data. Norwegian Journal of Geology, 92, 377-389.

Baranowski S., 1968, Thermic conditions of the periglacial tundra in SW Spitsbergen, Acta Universitas Wratislaviensis 68, Studia geograficzne X (in Polish with Eng. abstract), pp.74

Carcione J., Seriani G., 2001, Wave Simulation in Frozen Porous Media, Journal of Computational Physics, 170, 676–695, doi:10.1006/jcph.2001.6756

Christiansen H.H., Etzelmüller B., Isaksen K., Juliussen H., Farbrot H., Humlum O., Johansson M., Ingeman-Nielsen T., Kristensen L., Hjort J., Holmlund P., Sannel A.B.K., Sigsgaard C., Åkerman H.J., Foged N., Blikra L.H., Pernosky M.A., Ødegård, R.S., 2010, The thermal state of permafrost in the Nordic area during the international polar year 2007–2009. Permafrost and Periglacial Processes, 21, 156–181.

Christiansen H.H., Gilbert GL., Demidov N., Guglielmin M., Isaksen K., Osuch M., Boike J., 2019a, SESS Report 2019 - The State of Environmental Science in Svalbard, Svalbard Integrated Arctic Earth Observing System, Longyearbyen.

Christiansen H.H., Gilbert G.L., Demidov N., Guglielmin M., Isaksen K., Osuch M., Boike J., 2019b, Permafrost thermal snapshot and active-layer thickness in Svalbard 2016–2017. In: Orr (Eds), SESS Report 2018, Svalbard Integrated Arctic Earth Observing System, Longyearbyen, pp. 26 – 47.

Christiansen H.H., Gilbert G.L., Demidov N., Guglielmin M., Isaksen K., Osuch M., Boike J., 2020, Permafrost temperatures and active layer thickness in Svalbard during 2017/2018 (PermaSval). In: Van den Heuvel (Eds), SESS Report 2019, Svalbard Integrated Arctic Earth Observing System, Longyearbyen, pp. 236 –249.

Christiansen H. H., Gilbert G. L., Neumann U., Demidov N., Guglielmin M., Isaksen K., Osuch M., Boike J., 2021, Ground ice content, drilling methods and equipment and permafrost dynamics in Svalbard 2016–2019 (PermaSval) , doi: 10.5281/zenodo.4294095

Czerny J., Kieres A., Manecki M., Rajchler J., 1993, Geological Map of the SW part of Wedel Jarlsberg Land, Spitsbergen, 1:25000, Institute of Geology and Mineral Deposits, Kraków.

Dobiński W., 2011, Permafrost in the selected areas of Tatra Mts, the Scandinavian Mts, and Spitsbergen in the light of extensive geophysical studies and climatological analyses, Prace naukowe Uniwersytetu Śląskiego w Katowicach nr 2850, Wydawnictwo Uniwersytetu Śląskiego (in Polish with English and German summary).

Dobiński W., 2020, Permafrost active layer, Earth-Science Reviews, 208, 103301, doi: /10.1016/j.earscirev.2020.103301

455 Dobiński W., Leszkiewicz J., 2010, Active layer and permafrost occurrence in the vicinity of the Polish
456 Polar Station, Hornsund, Spitsbergen in the light of geophysical research, Problemy Klimatologii
457 Polarnej, 20, 129–142 (in Polish with English summary).

458 Dolnicki P., 2005, Spatial distribution of permafrost level and its connection with variable
459 disap–pearance snow cover in the area of Fuglebergsletta (SW Spitsbergen), Polish Polar Studies.XXXI
460 Sympozjum Polarne, Kielce, 34–45 (in Polish)

461 Dolnicki P., 2010, Changes of thermic of the ground in Hornsund (SW Spitsbergen) in the period 1990–
462 2009, Problemy Klimatologii Polarnej, 20, 121-127 (in Polish with English summary)

463 Dolnicki P., Grabiec M., Puczko D., Gawor Ł. , Budzik T. , Klementowski J., 2013, Variability of
464 temperature and thickness of permafrost active layer at coastal sites of Svalbard, Polish Polar Res., 34,
465 4, 353-374

466 Dou S., Ajo-Franklin J.B., 2014, Full-wavefield inversion of surface waves for mapping embedded low-
467 velocity zones in permafrost, Geophysics, 79, 1ND-Z201, doi: 10.1190/geo2013-0427.1

468 Draebing D., 2016, Application of refraction seismics in alpine permafrost studies: A review, Earth-
469 Science Reviews, 155, 136–152.

470 Draebing D., Krautblatter M., 2012, P-wave velocity changes in freezing hard low-porosity rocks: a
471 laboratory-based time-average model. The Cryosphere, 6, 1163–1174.

472 Gido N.A.A., Bagherbandi M., Sjöberg L.E., Tenzer R., 2019, Studying permafrost by integrating satellite
473 and in situ data in the northern high-latitude regions, Acta Geophysica, 67, 721–734, doi:
474 10.1007/s11600-019-00276-4

475 Glazer M., Dobiński W., Marciniak A., Majdański M., Błaszczyk M., 2020, Spatial distribution and
476 controls of permafrost development in non-glacial Arctic catchment over the Holocene, Fuglebekken,
477 SW Spitsbergen, Geomorphology, 358, 107128.

478 Gregersen O., Phukan A., Johansen T., 1983, Engineering properties and foundations design
479 alternatives in marine Svea clay, Svalbard. Permafrost, Fourth International Conference Proceedings,
480 National Academy Press Washington D.C.

481 Grześ M., 1984, Characteristics of the active layer of permafrost in Spitsbergen, XI Sympozjum Polarne,
482 Poznań, 65–83 (in Polish)

483 Hauck C., Kneisel C., 2009, Applied Geophysics in Periglacial Environments, Cambridge University Press,
484 doi: 10.1017/CBO9780511535628

485 Hilbich C., 2010, Time-lapse refraction seismic tomography for the detection of ground ice
486 degradation, The Cryosphere, 4, 243–259.

487 Hobro J.W.D., Singh S.C., Minshull T.A., 2003, Three-dimensional tomographic inversion of combined
488 reflection and refraction seismic traveltime data, Geophysical Journal International, 152, 79–93.

489 Humlum O., Instanes A., Sollid J.L., 2003, Permafrost in Svalbard: a review of research history, climatic
490 background and engineering challenges, Polar Research, 22, 191–215.

491 IPCC, 2019: Climate Change and Land: an IPCC special report on climate change, desertification, land
492 degradation, sustainable land management, food security, and greenhouse gas fluxes in terrestrial
493 ecosystems [P.R. Shukla, J. Skea, E. Calvo Buendia, V. Masson-Delmotte, H.-O. Pörtner, D. C. Roberts,
494 Zhai P., Slade R., Connors S., van Diemen R., Ferrat M., Haughey E., Luz S., Neogi S., Pathak M., Petzold
495 J., Portugal Pereira J., Vyas P., Huntley E., Kissick K., Belkacemi M., Malley J., (eds.)]. In press.

496 Johansen T.A., Digranes P., van Schaak M., Lonne I., 2003, Seismic mapping and modeling of near-
497 surface sediments in polar areas, Geophysics, 68, 566-573.

498 Johansen T.A., Ruud B.O., Bakke N.E., Riste P., Johannessen E.P., Henningsen T., 2011, Seismic profiling
499 on Arctic glaciers, First Break, 29, 65-71.

500 Jahn A., 1982, Soil thawing and active layer of permafrost in Spitsbergen, Acta Universitatis
501 Wratislaviensis 525, Spitsbergen Expeditions IV, pp. 57-75

502 Jahn A., 1988, Periglacial soil structures in Spitsbergen and in central Europe, V International
503 Conference on Permafrost, Trondheim, 769–800

504 Kasprzak M., 2015, High-resolution electrical resistivity tomography applied to patterned ground,
505 Wedel Jarlsberg Land, south-west Spitsbergen, Polar Research 34, 25678.

506 Kasprzak M., 2020, Seawater intrusion on the Arctic coast (Svalbard): The concept of onshore-
507 permafrost wedge, Geosciences, 10, 349, doi: 10.3390/geosciences10090349

508 Kasprzak M., Strzelecki M.C., Kondracka M., Traczyk M., Kondracka M., Lim M., Migała K., 2017, On the
509 potential for a bottom active layer below coastal permafrost: the impact of seawater on permafrost
510 degradation imaged by electrical resistivity tomography (Hornsund, SW Spitsbergen), Geomorphology,
511 293, 347–359.

512 Lecomte I., Polom U., Sauvin G., Ruud B.O., Christiansen H., Gilbert G., 2014, Shear-wave Reflection-
513 seismic Pilot Study at the UNIS C02 Lab site, Longyearbyen, Svalbard. 76th EAGE Conference
514 Proceedings, WE P04 05, 5 pp.

515 Leszkiewicz J., Caputa Z., 2004, The thermal condition of the active layer in the permafrost at Hornsund,
516 Spitsbergen, Polish Polar Research, 25, 223–239.

517 Marciniak A., Stan-Kłeczek I., Idziak A., Majdański M., 2019, Uncertainty based multi-step seismic
518 analysis for near-surface imaging, Open Geosciences, 11, 727-737.

519 Marsz A.A., Styszynska A., Pekala K., Repelewska-Pekalowa J., 2013, Influence of meteorological
520 elements on changes in active-layer thickness in the Bellsund region, Svalbard, Permafrost and
521 Periglacial Processes, 24, 304–312.

522 Miętus M., 1988, Short period changes of soil temperature against advective changes of air
523 temperature in Hornsund, Spitsbergen, Polish Polar Research, 9, 95–103.

524 Miętus M., Filipiak J., 2001, Variability of ground temperature in Hornsund in the period 1979−1999.
525 Przegląd Geofizyczny, 46, 4, 323–337 (in Polish).

526 Migała K., 1991, Effect of winter season and snow cover on the active layer of permafrost in the region
527 of Hornsund (SW Spitsbergen), Wyprawy Geograficzne na Spitsbergen, Lublin, 248. (in Polish)

528 Migała K., 1994, The characteristic features of the active layer of the permafrost in the climate of
529 Spitsbergen, Acta Universitatis Wratislaviensis 1590, Prace Instytutu Geograficznego C, Meteorologia i
530 Klimatologia, 1, pp. 79-111 (in Polish with Eng. abstract)

531 Millero F. J., Feistel R., Wright D. G., McDougall T. J., 2008, The composition of Standard Seawater and
532 the definition of the Reference-Composition Salinity Scale, Deep Sea Research Part I: Oceanographic
533 Research Papers, 55, 1, 50-72

534 Minsley B. J., Abraham J.D., Smith B.D., Cannia J.C., Voss C.I., Jorgenson M.T., Walvoord M.A., Wylie
535 BK., Anderson L., Ball L.B., Deszcz-Pan M., Wellman T.P., Ager T.A., 2012, Airborne electromagnetic
536 imaging of discontinuous permafrost, Geophysical Research Letters, 39, L02503,
537 doi:10.1029/2011GL050079

538 Osuch M., Wawrzyniak,T., Nawrot, A., 2019, Diagnosis of the hydrology of a small Arctic permafrost
539 catchment using HBV conceptual rainfall-runoff model, Hydrology Research, 50, 459–478.

540 Owoc B., Górszczyk A., Majdański M., 2018, The discussion of the uncertainty in the traveltime seismic
541 tomography, EAGE conference proceedings, TU 24P2 04, 5 pp.

542 Oye V., Braathen A., Polom U., 2013, Preparing for CO2 storage at the Longyerbyen CO2 Lab:
543 microseismic monitoring of injection tests, First Break, 31, doi: 10.3997/1365-2397.31.7.70361.

544 Park C.B., Miller R.D., Xia J., 1999, Multichannel analysis of surface waves, Geophysics, 64, 800-808.

545 Pękala K., Repelewska-Pękalowa J., 1990, Relief and stratigraphy of Quaternary deposits in the region
546 of Recherche Fjord and southern Bellsund (Western Spitsbergen), Wyprawy Geograficzne na
547 Spitsbergen, UMCS, Lublin, Poland.

548 Rachlewicz G., Szczuciński, W., 2008, Changes in thermal structure of permafrost active layer in a dry
549 polar climate, Petuniabukta, Svalbard, Polish Polar Research, 29, 261–278.

550 Rossi G., Accaino F., Boaga J., Petronio L., Romeo R., Wheeler W., 2017, Seismic survey on an open
551 pingo system in Adventdalen Valley, Spitsbergen, Svalbard, Near Surface Geophysics, 16, 89-103,
552 doi:10.3997/1873-0604.2017037

553 Schrott L., and Hoffmann T., 2008, Refraction seismics, Cmabridge University Press, 57-80,
554 doi:10.1017/CBO9780511535628.004

555 Sobota I., Nowak M., 2014, Changes in the dynamics and thermal regime of the permafrost and active
556 layer of the High Arctic coastal area in north-west Spitsbergen, Svalbard. Geografiska Annaler: Series
557 A, Physical Geography, 96, 227–240.

558 Strobbia C., Glushchenko A., Laake A., Vermeer P., Papworth T.J., Ji Y., 2009, Arctic near surface
559 challenges: the point receiver solution to coherent noise and statics, First Break, 27.

560 Tsuji T., Johansen T.A., Ruud B.O., Ikeda T., Matsuoka T., 2012, Surface-wave analysis for identifying
561 unfrozen zones in subglacial sediments, Geophysics, doi: 10.1190/geo2011-0222.1

562 Wawrzyniak T., Osuch M., Napiórkowski J., Westermann S., 2016, Modelling of the thermal regime of
563 permafrost during 1990–2014 in Hornsund, Svalbard. Polish Polar Research, doi: 10.1515/popore-
564 2016-0013

565 Wawrzyniak T., Osuch M., 2020, A 40-year High Arctic climatological dataset of the Polish Polar Station
566 Hornsund (SW Spitsbergen, Svalbard), Earth System Science Data, 12, 805–815, doi:/10.5194/essd-12-
567 805-2020

568 Wawrzyniak T., Majerska M., Osuch M., 2021, Hydrometeorological dataset (2014–2019) from the high
569 Arctic unglaciated catchment Fuglebekken (Svalbard), Hydrological Processes, 35:e13974, doi:
570 10.1002/hyp.13974

571

572 Figure Captions:

573 Fig. 1 Digital terrain map of the study area in the Fuglebekken catchment nearby the Polish Polar
574 Station in Hornsund (PSPH, red box). The locations of the two seismic surveys are marked: Unfrozen
575 survey in October 2017 (red) and Frozen survey in April 2018 (blue). Both lines match the previous ERT
576 survey. Numbers 1-3 mark the position of shallow boreholes with thermal and piezometer
577 measurements. Borehole 2 lies 50 m and 3 lies 250 m out-of-the-line in the position of previous
578 monitoring sites. Insets show the position of Svalbard (left) and Hornsund (right).

579 Fig. 2 Daily mean air temperature at the meteorological station in the PSPH (top) with marked time
580 (dashed lines) of both surveys: in Frozen condition (blue) and Unfrozen conditions (red). Continuous
581 ground temperature measurements were recorded in three boreholes (see inset for a location with
582 marked closest points on the line). Clear seasonal variation was observed. The time of both seismic
583 surveys (red and blue dashed lines) is marked. The next unfrozen line marks the time in the consecutive
584 year showing similar thermal conditions in which seismic Frozen survey was acquired.

585 Fig. 3 Schematic geometry of both seismic fieldwork arrangements. Elevation along the profile (top)
586 with the position of boreholes marked, acquisition geometry in two seasons: Unfrozen (middle) in
587 2017, Frozen (bottom) in 2018. The survey in 2018 used 5-m receiver spacing, resulting in much larger
588 offsets (up to 350 m).

589 Fig. 4 Example of seismic wavefield recorded at the same shot location (shot position 142 m) in the
590 two seasons: unfrozen (top) and frozen (bottom). Clear P and S wave refractions and wide-angle
591 reflections are visible. No surface waves were recorded in frozen conditions. The table presents
592 refraction velocities measured at large offsets showing a significant change in apparent velocities.

593 Fig. 5 Results of surface waves dispersion analysis (MASW) for unfrozen survey data: 1D models for
594 areas are marked with black triangles (top); 2D interpolation (bottom). Main S-wave velocity change
595 (300 to 1300 m/s) is identified as the sediments-bedrock boundary, shallow smaller change (200 to
596 300 m/s) corresponds to the interpreted groundwater table. Vertical lines mark MASW depth
597 uncertainty. No surface waves were observed in the frozen survey.

598 Fig. 6 Shallow P wave velocity distribution from the unfrozen survey, based on 1D fit at regular
599 intervals, marked with triangles (top), and 2D short offset seismic refraction (bottom). The velocity
600 jump at about 10 m depth (1500 to 3500 m/s) corresponds to bedrock depth.

601 Fig. 7 Seismic refraction (a, b) and ray-based tomography results (c, d) for both seasons: unfrozen 2017
602 (left) and frozen 2018 (right). The uncertainty of the tomography (e, f) shows the significance of the
603 results down to 30 m. Higher velocities are visible at a depth of 30 m in the frozen survey.

604 Fig. 8 Schematic interpretation of seismic velocity and thermal structures. The grey line marks the
605 lithological boundary between fluvial sediments and bedrock. The numbers show the velocities of P
606 and S waves observed in the unfrozen (red) and frozen (blue) surveys. The previous ERT result (top,
607 after Glazer et al. 2020). Insets show thermal profiles of the three boreholes in the vicinity. Black
608 dashed lines mark the range of the influence of seawater on freezing in sediments. A thick dashed line
609 marks the deep fault recognized in the area.

610

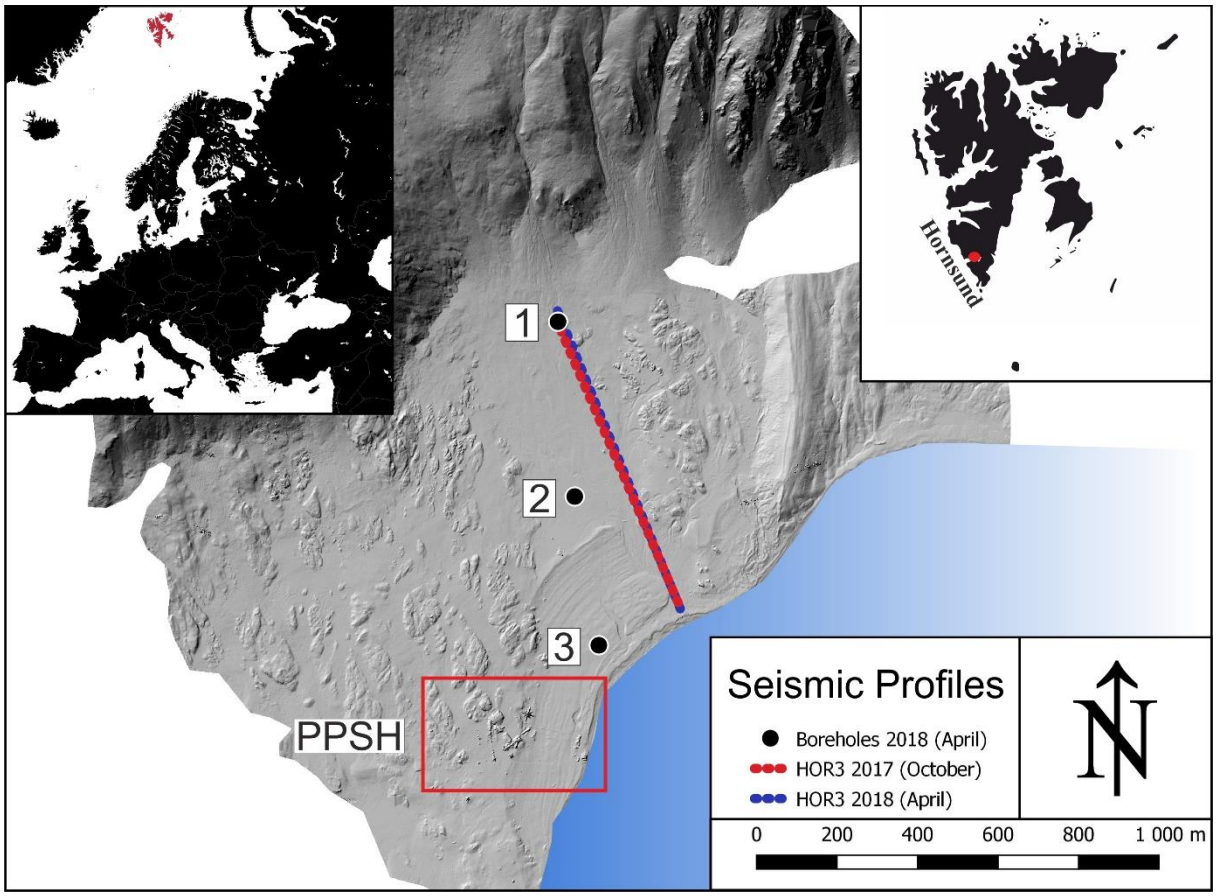

611

612 Fig. 1

613

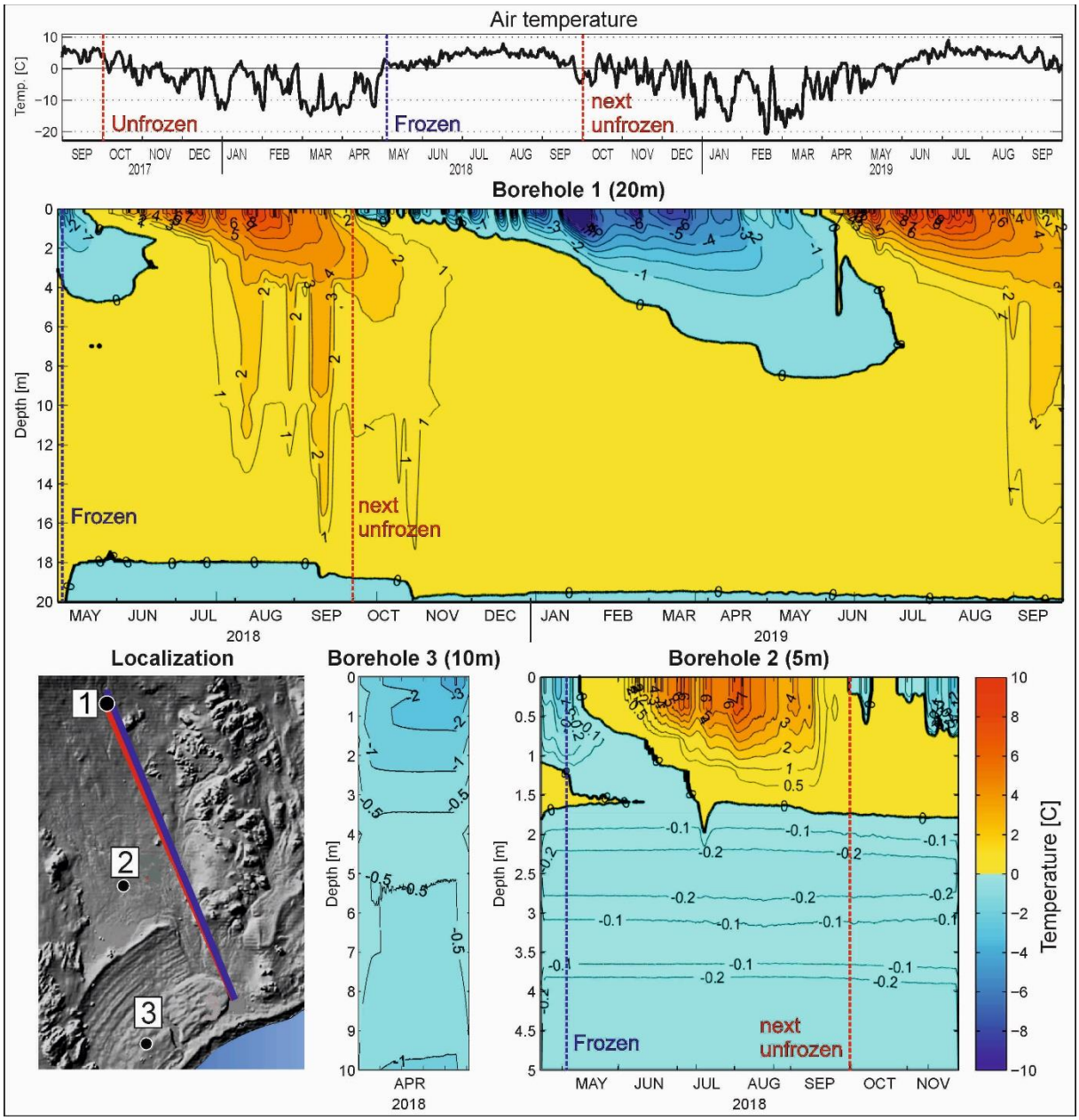

614

615 Fig. 2

616

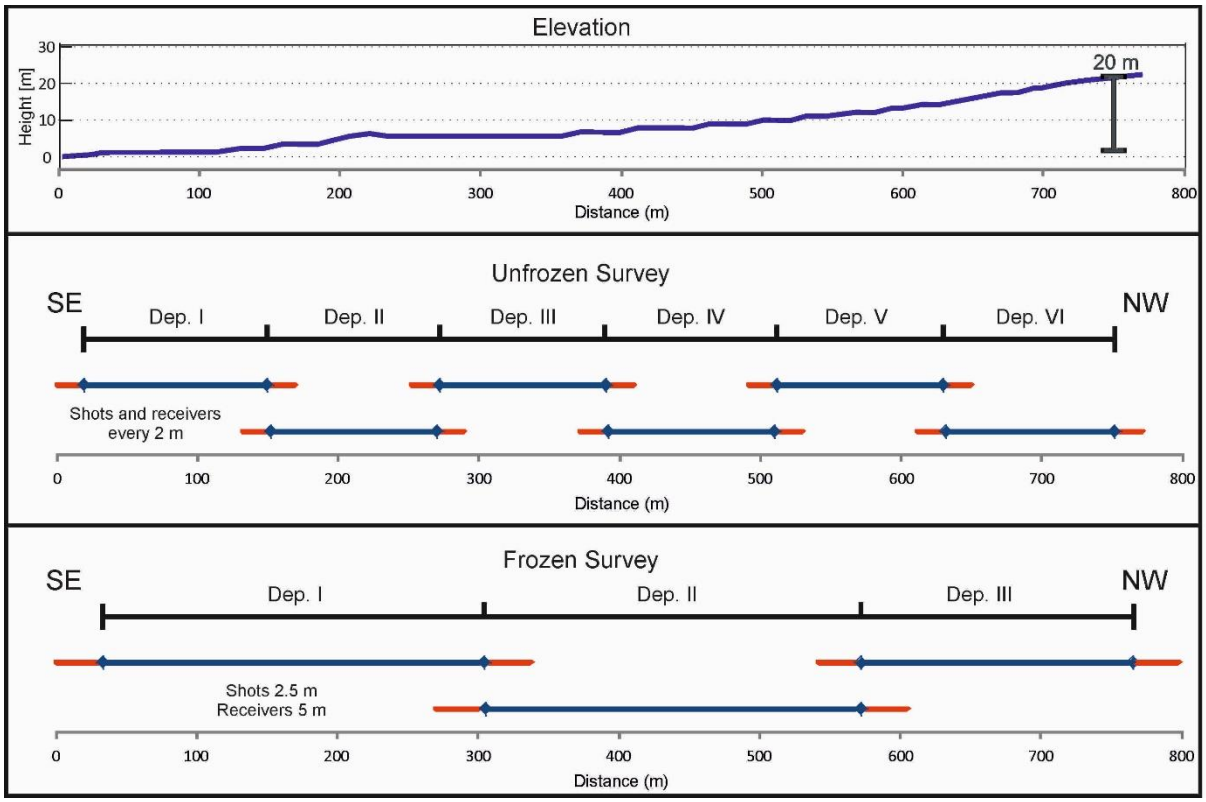

617

618 Fig. 3

619

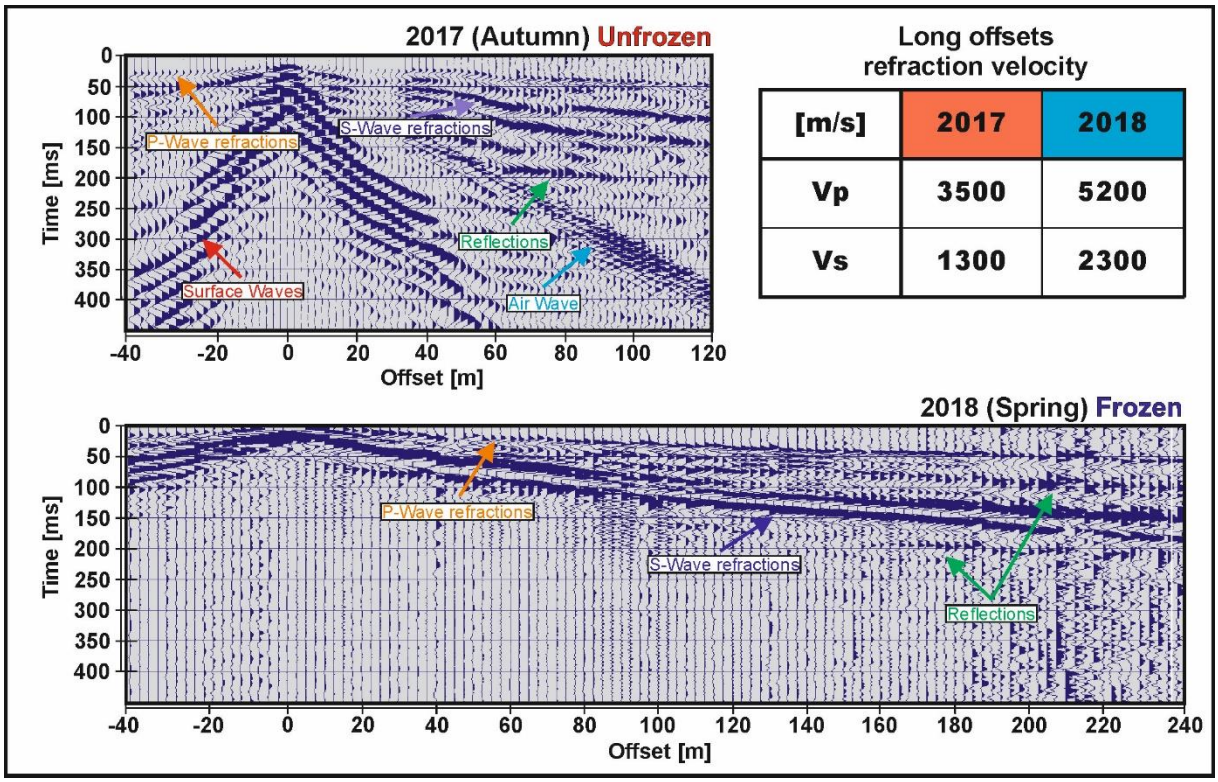

620

621 Fig. 4

622

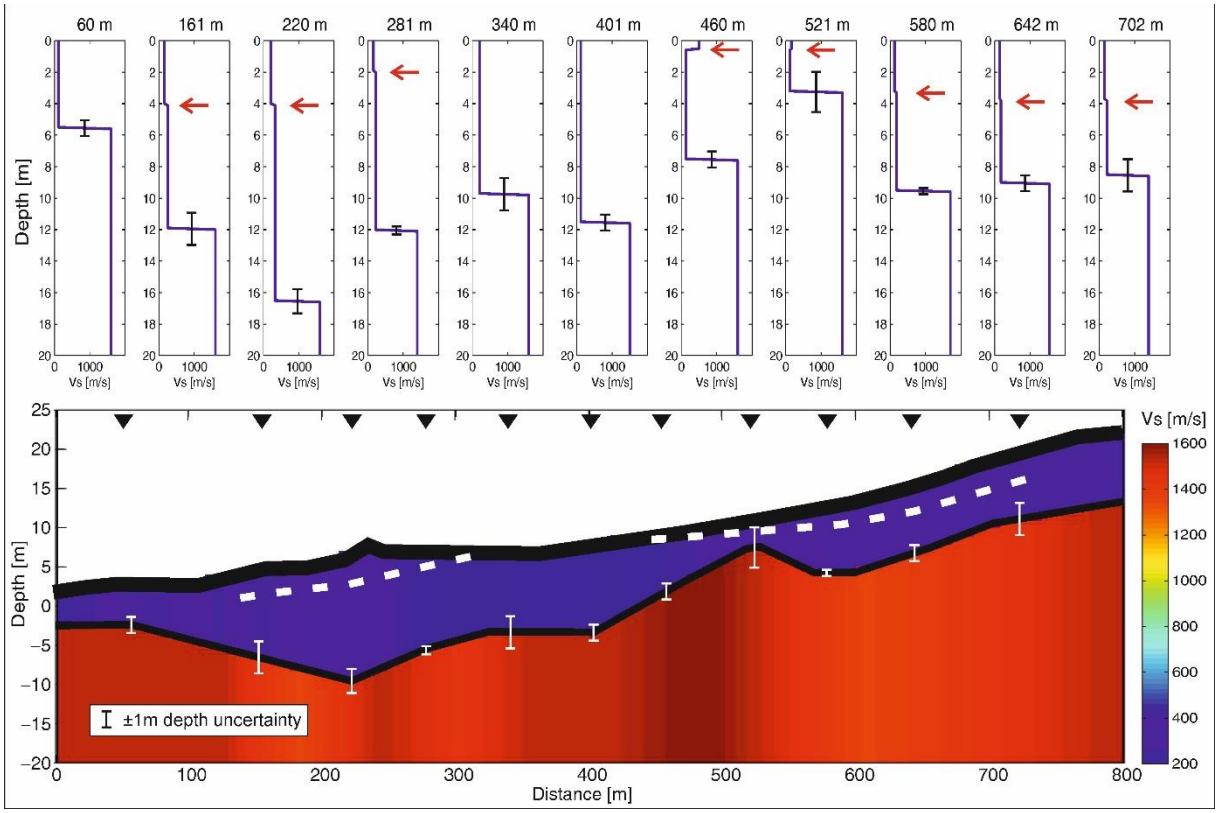

623

624 Fig. 5

625

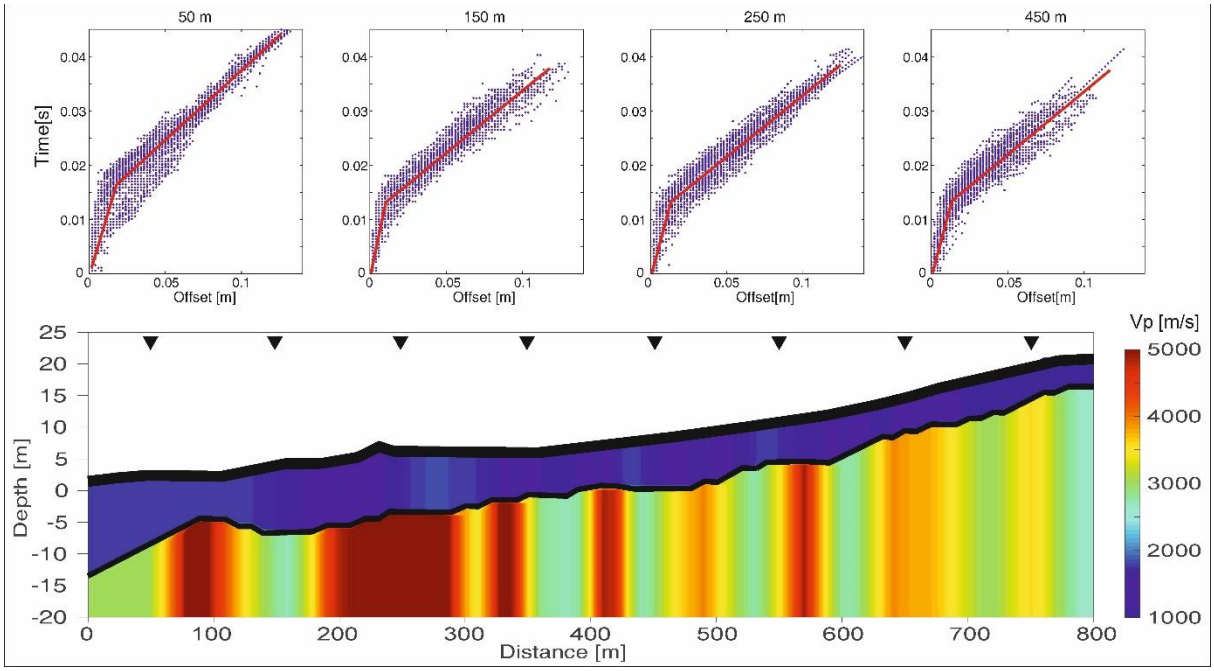

626

627 Fig. 6

628

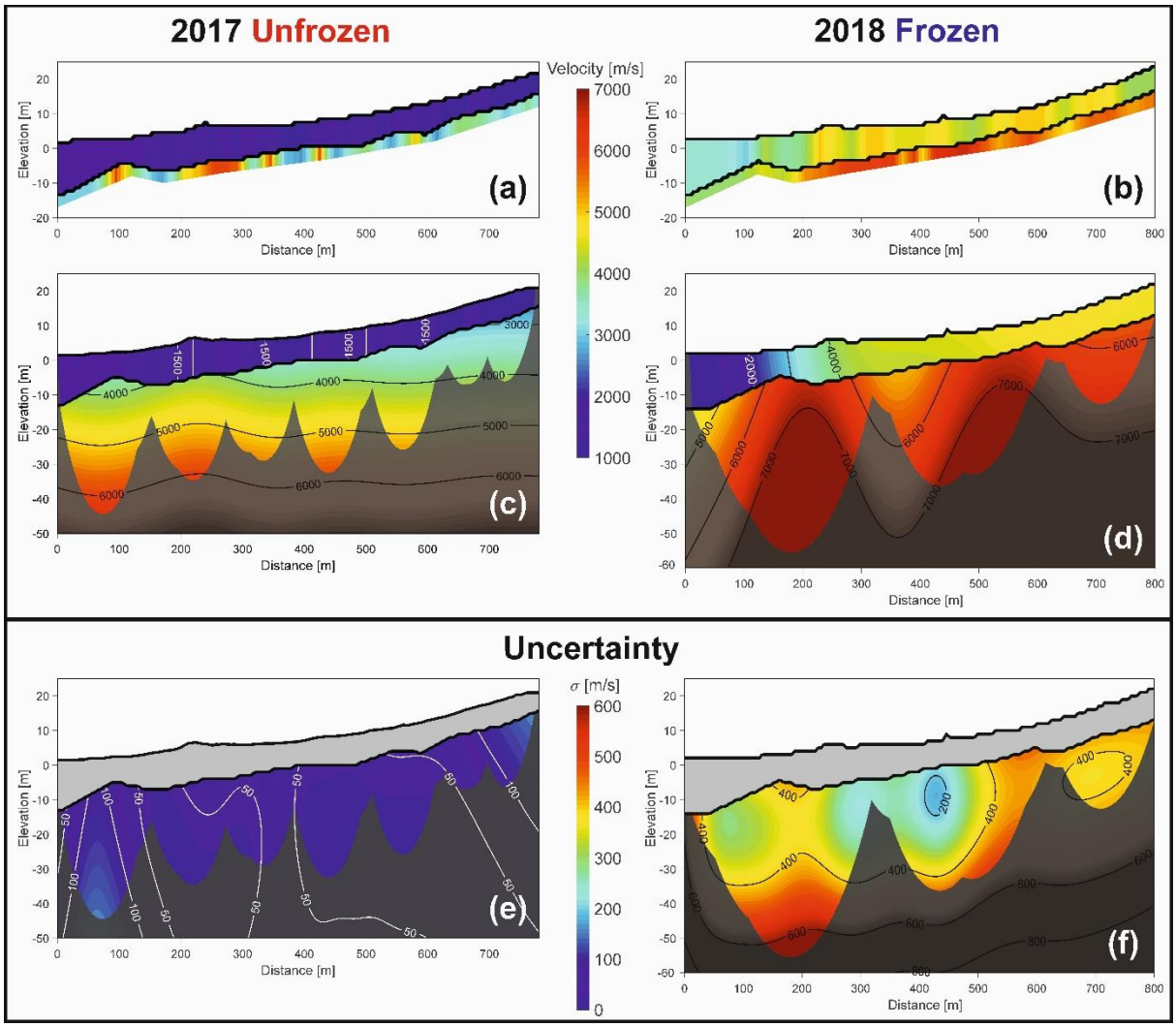

629

630 Fig. 7

631

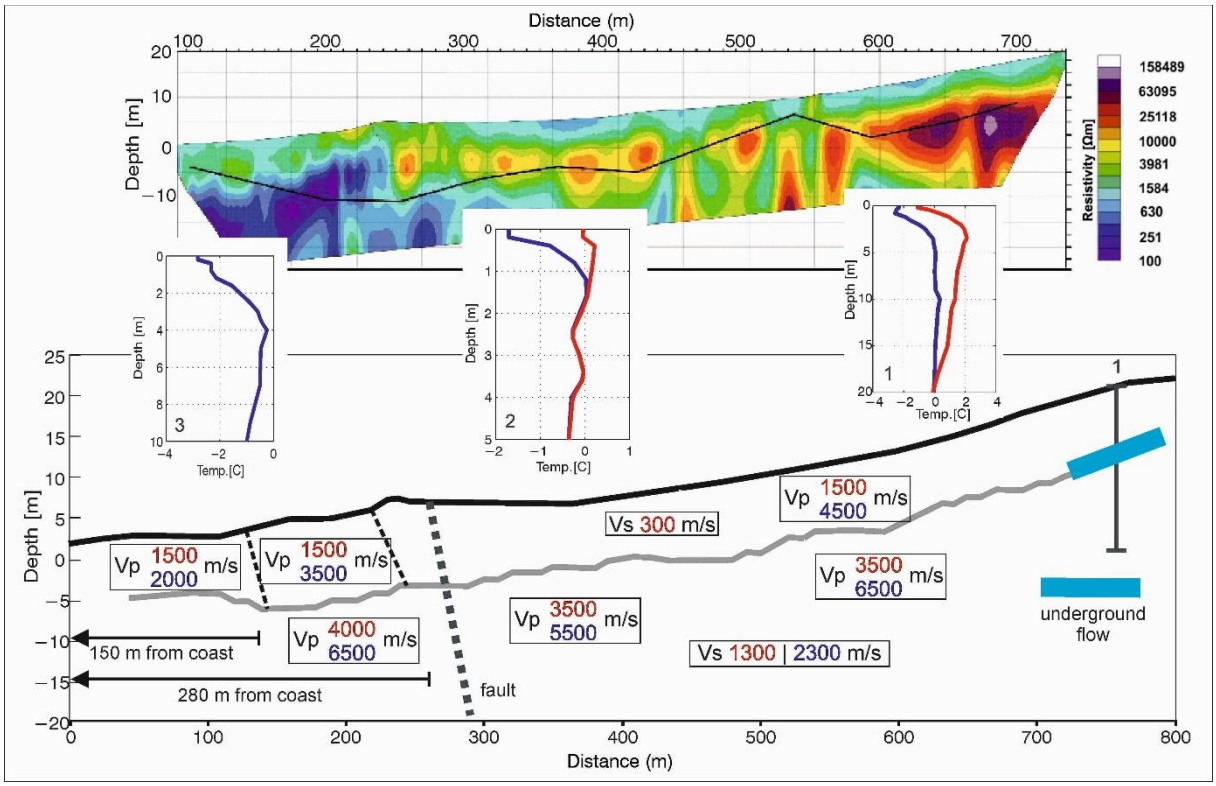

632

633 Fig. 8

634